

# ALUMINOSILICATE DIAGENESIS IN A TERTIARY SANDSTONE-MUDROCK SEQUENCE FROM THE CENTRAL NORTH SEA, UK

J. M. HUGGETT

*Department of Geology, Imperial College of Science, Technology and Medicine, London, SW7 2BP, UK*

*(Received 24 November 1995; revised 20 March 1996)*

**ABSTRACT:** Mudrocks and sandstones from the Palaeocene of the central North Sea have been studied to assess the petrology, diagenesis and extent of any chemical interaction between the two lithologies. Authigenic and detrital minerals have been distinguished using a variety of electron microscope techniques. Small but significant quantities of authigenic minerals, which would not be detected by conventional petrographic tools, have been detected through the use of high-resolution electron beam techniques. Sandstone mineralogy has been quantified by point counting, and mudrock mineralogy semi-quantified by XRD. The detrital and authigenic mineralogy in the sandstone is almost identical to that found in the mudrock. The principal difference is in the relative proportions. Qualitative mass balance suggests that cross-formational flow has not been significant in either clay or quartz diagenesis.

Researchers attempting to quantify the diagenetic relationship between mudrocks and sandstones have concluded that mudrocks act as closed systems (e.g. Hower *et al.*, 1976; Pearson & Small, 1988; Totten & Blatt, 1993) or that reactants move freely between the two lithologies (e.g. Curtis, 1978; Boles & Franks, 1979; Awwiller, 1993). Until recently, X-ray diffraction (XRD) has been the principal investigative tool in mudrock diagenesis. Consequently, identification of authigenic minerals has been by inference rather than by observation. Numerous transmission electron microscopy/analytical electron microscopy (TEM/AEM) studies have investigated illite-smectite diagenesis, but not in the broader context of mudrock diagenesis. In this study, a combination of electron microscope techniques, optical microscopy and XRD have been used to examine the mineralogy of interbedded marine sandstones and mudrocks, buried to ~2.3 km. In particular, an attempt has been made to establish whether there has been any exchange of ionic transfer between the two lithologies.

The sediments described are from a proximal turbidite fan sequence which prograded from west to east into the UK sector of the central North Sea.

## SAMPLE MATERIAL

The sampled interval is a cored Palaeocene sandstone dominated sequence from a well in the UK sector of the central North Sea. The overall ratio of sandstone to mudrock is high, ~84%, and individual mudrock beds average ~0.3 m thick. A single mudrock unit 30 m thick occurs near the base of the sampled interval. Although Palaeocene sequences of the North Sea are known to have a high volcanogenic component and numerous water-lain tuffs are recorded elsewhere (Knox & Morton, 1988), in this sequence no lithologically discrete volcanogenic beds were identified.

The sequence has undergone a simple continuous burial history since deposition and now lies between 2200 and 2300 m. The present-day average formation temperature, based on TD logging bottom hole temperature, is 107°C.

## METHODS

Whole-rock and <4 µm clay fraction XRD analyses were carried out on 31 mudrock samples and 11 sandstone samples. The clay fraction samples were prepared by suction onto ceramic tiles (Shaw, 1972). Samples were scanned on a Philips 1820

automated X-ray diffractometer using Ni-filtered Cu-K $\alpha$  radiation. The operating conditions used and methods for semi-quantitative determinations of mineral components are described in Huggett (1992). Semi-quantitative data are accurate to within  $\sim 10\%$  of quoted values; this assessment of accuracy is based on repeated analysis of known mixtures of standard clays (which will not necessarily produce identical profiles to the mixtures of detrital and authigenic clays in natural mixtures).

The abundant illite in the mudrock precluded use of the precise method of Śródoń (1980) for identification of the proportion of smectite in illite-smectite. The presence of low-angle illite-smectite superlattice reflections precluded use of the method of Śródoń (1981) for determining the proportion of smectite in illite-smectite because the method is only applicable to smectite-rich randomly interstratified illite-smectite. Estimates of the illite-smectite composition were therefore obtained from measurement of the glycol-treated 002/003 reflection (where it could be clearly identified) after peak deconvolution to separate out the discrete illite component (Moore & Reynolds, 1989).

Forty-five sandstone samples were examined using an optical microscope. Proportions of major components were estimated but no point count data are available. Samples for petrological analysis in back-scattered electron imaging (BEI) mode were prepared by gently polishing rock chips which had been vacuum impregnated with low viscosity araldite. The polished samples were examined in a Hitachi S2500 SEM with an Oxford Instruments 860 EDS analyser. Semi-quantitative and quantitative energy dispersive X-ray analyses were carried out to characterize silt-size particles. Ten sandstone samples were examined by fracture-surface SEM, with qualitative EDS to confirm mineral identifications. The relatively low resolution of backscattered electron microscopy (BSEM) is typically  $\times 3000$ , which precludes the obtaining of much useful morphological data on clays in mudrocks. However, with a field emission SEM (FESEM), magnifications of 20,000–50,000 are routine. Fresh fracture surfaces were platinum coated for FESEM examination. Qualitative EDS analyses were carried out in the FESEM using an Oxford Instruments high-purity germanium detector with Moran Scientific software.

Mudrock samples for TEM were prepared by ion-beam milling and by ultra-microtomy; see Phakey *et al.* (1972) for details of the former technique,

Tessier & Pedro (1982) for the latter. The samples for ion-milling were cut from 30  $\mu\text{m}$  thick thin-sections cut normal to bedding so that the phyllosilicate 001 orientations were preferentially parallel to the electron beam. Samples for ultramicrotomy were imbedded in medium-hard resin and sectioned using a Reichert Jung Ultracut E. Duplicate samples from several depths were prepared by the method devised by Tessier (described in Śródoń *et al.*, 1990) for fixing smectite layers at 12.5–15 Å. All TEM samples were examined in a Jeol 4000FX TEM. Lattice fringe measurements were made in the Scherzer underfocus condition to obtain structural information (Guthrie & Veblen, 1989). Semi-quantitative EDS analyses were obtained from single particles using a Philips T200 with an Oxford Instruments lithium drifted silicon detector and AN10000 software.

## SANDSTONE PETROLOGY

### *Detrital mineralogy*

The sandstones are quartz-dominated with subordinate amounts of feldspar, rock fragments and clay matrix. Other detrital components include biotite (variably altered to chlorite), muscovite, heavy minerals, glauconite, organic matter, plus very rare bioclasts and chlorite grains.

The proportion of mica decreases with depth, from  $<5\%$  to  $<1\%$ . Detrital clay matrix (probably mostly illite and illite-smectite) forms a variable proportion of the sandstones, but is typically  $<5\%$ . The XRD data show no depth trend in the proportions of illite or illite-smectite (Fig. 1). Visible porosity is 5–20% and predominantly intergranular, some of which may be secondary, generated through leaching of ferroan calcite. On average, an estimated 1% of the porosity was generated by feldspar leaching (mostly K-feldspar), and  $<0.5\%$  through rock fragment leaching (principally tuff and chert). Organic content is typically  $\leq 1\%$  (mean = 0.4%), but ranges up to 3%.

### *Authigenic non-clay minerals*

The paragenetic sequence, so far as it has been established, is summarized in Fig. 2. The principal authigenic minerals in the sandstones are ferroan calcite and quartz overgrowth. The total proportion of non-clay authigenic minerals is typically  $<3\%$ .

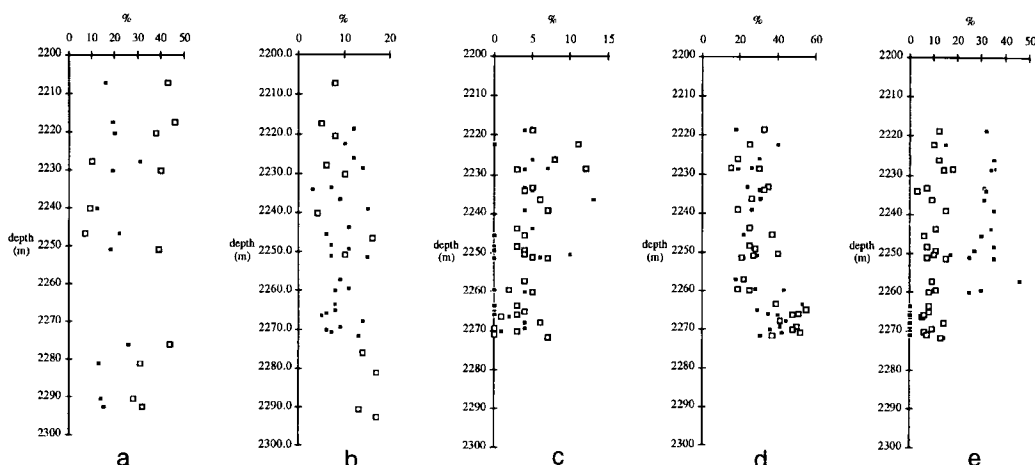


FIG. 1. (a) Depth plotted against semi-quantitative percentages for illite (solid squares) and illite-smectite (open squares) in the  $<4\ \mu\text{m}$  fraction of selected sandstone samples. (b) Depth plotted against chlorite semi-quantitative percentages ( $<4\ \mu\text{m}$  fraction XRD data). Mudrock (solid squares), sandstone (open squares). (c) Depth plotted against semi-quantitative percentages of plagioclase and K-feldspar in the mudrocks. Solid squares = K-feldspar, open squares = plagioclase. (d) Depth plotted against semi-quantitative percentages for illite (solid squares) and illite-smectite (open squares) in the mudrock  $<4\ \mu\text{m}$  fraction. Data points are accurate to within 10% of the plotted values. (e) Depth plotted against semi-quantitative percentages for kaolinite (solid squares) and chlorite (open squares) in the mudrock  $<4\ \mu\text{m}$  fraction. Data points are accurate to within 10% of the plotted values in 1 a–e.

From textural data the quartz and carbonate cements are inferred to be relatively early, with the quartz predating the carbonate.

Ferroan calcite is present as small concretions and stratabound cement layers 0.5–1.5 m thick. Together these form 25–40% cement in 3% of the total sandstone thickness cored. Matrix clay has been replaced by ferroan calcite, whilst quartz and feldspar grains are very slightly corroded by ferroan calcite (although the rare calcite bioclasts are not). Ferroan calcite spar formed after kaolinite, pyrite and quartz overgrowth cements.

#### *Authigenic kaolinite*

Kaolinite is a minor but ubiquitous component in the sandstones ( $<1\%$ ). It has not been possible to determine which polymorph is present from the XRD data, though several data points suggest that a mixture of kaolinite and dickite may be present. Kaolinite is subhedral throughout and mostly relatively coarse grained (10–15  $\mu\text{m}$ ) pore-filling aggregates and vermicules, with some coarser pseudomorphs after mica. Aggregates of denser

packed, finer (5–10  $\mu\text{m}$ ) kaolinite platelets occur in some samples. These may represent a separate episode of kaolinite formation. Kaolinite has also replaced argillized tuff fragments, and more rarely, plagioclase. Kaolinite predates ferroan calcite, and overlaps with pyrite and quartz overgrowth.

#### *Authigenic chlorite*

The XRD data for the  $<4\ \mu\text{m}$  fraction (Fig. 1b) indicate that authigenic chlorite increases slightly with depth. The chlorite is a mixture of detrital, silt-size flakes, coarsely crystalline aggregates which may have replaced biotite (Fig. 3) and authigenic, Fe-rich clay-grade aggregates of platelets, and occurs as occasional radial grain coatings and intimately intergrown with detrital clay. Authigenic kaolinite and chlorite occur together, without any evidence for the replacement of kaolinite by chlorite; from textural data alone it is difficult to assess which precipitated first. Like kaolinite, chlorite is slightly overgrown by quartz, suggesting that either the two co-precipitated, or the quartz formed later than the chlorite.

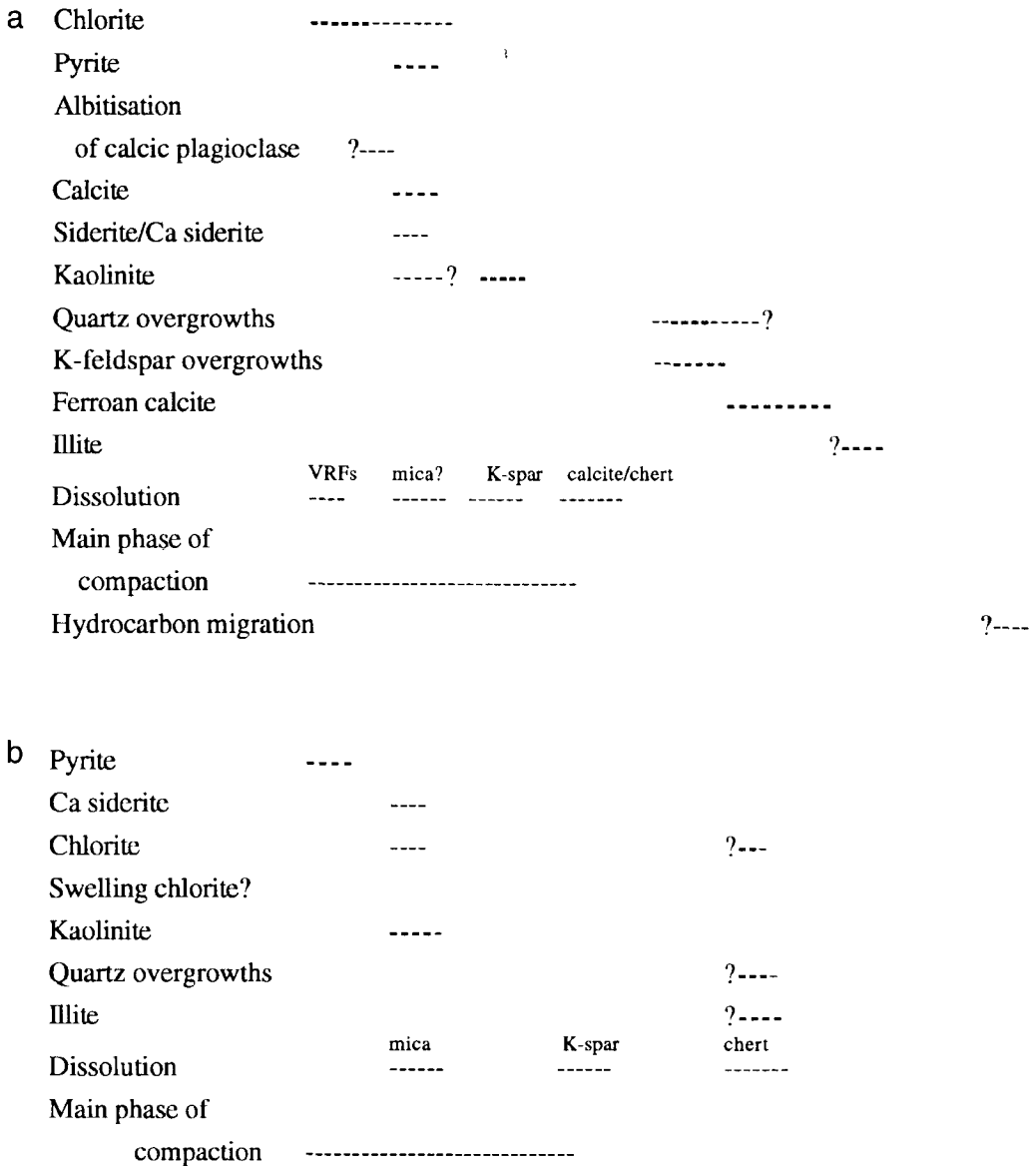


FIG. 2. (a) Sandstone diagenetic sequence (VRFs: volcanic rock fragments). (b) Mudrock diagenetic sequence.

### Authigenic illite

Short laths of authigenic clay are associated with detrital illitic clay, apparently as overgrowths to detrital platelets (Fig. 4a). The laths are too small to obtain EDS analyses sufficiently accurate to determine whether they are

illite or illite-smectite. However, for reasons given below, they are believed to be illite. Illite rests on quartz overgrowths, chlorite and kaolinite, though neither clay has been replaced by the authigenic illite. Visual estimates suggest  $\ll 1\%$  authigenic illite is present in the sandstones.

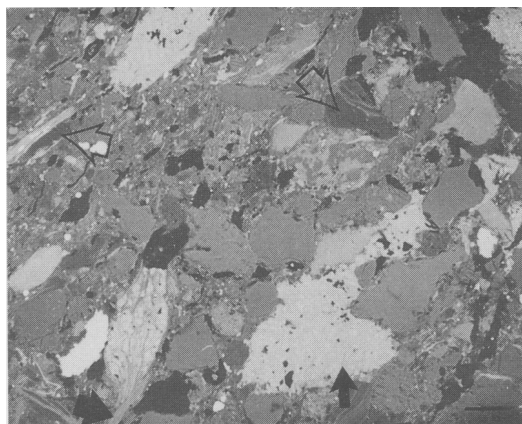


FIG. 3. Back-scatter electron micrograph of sandstone showing calcian siderite (white) intergrown with chlorite (pale grey, smallest arrow) and chlorite/mica intergrowth (large arrow), in which the chlorite is white, and the mica is pale grey. Dark grey aggregates are kaolinite, nucleated on, or replacing mica (open arrow). Sample depth = 2242.5 m; scale bar = 20  $\mu\text{m}$ .

## MUDROCK PETROLOGY

The mudrocks are mineralogically variable with no overall depth trend other than an absence of kaolinite between 2262.1 and 2271.28 m and an overall decrease in plagioclase with depth (Fig. 1c). Clay minerals constitute  $\sim 60\%$  of the mudrocks and are predominantly illite and illite-smectite (Fig. 1d), plus kaolinite and chlorite (Fig. 1e) and rare swelling chlorite (Fig. 5). In addition to clays, minor quartz, albite and cristobalite are present in the  $<4\ \mu\text{m}$  fraction. Non-clay minerals in the mudrocks are, in order of abundance, quartz, plagioclase (predominantly Ab-rich, same comments apply as to sandstone plagioclase), K-feldspar, minor lithic grains (schist, chert and polycrystalline quartz fragments) mica (mostly phengite), chlorite, pyrite, rare calcite, siderite, cristobalite and organic matter. Semi-quantitative XRD suggests that total feldspar is slightly less abundant in the mudrock than in the sandstones and that plagioclase (albite) is more abundant than K-feldspar (the reverse of the sandstones, Fig. 1c).

### *Illite and illite-smectite*

The XRD data for the mudrocks indicate that most of the clay is illite and illite-smectite,

typically 40–70% of the clay fraction (15–30% of the bulk rock), higher in the kaolinite-free interval (Fig. 1d). Estimates of the illite-smectite composition from the glycol-treated, deconvoluted 002/003 reflection were obtained for those samples with sufficient illite-smectite to produce a clear reflection after deconvolution (Fig. 5). These estimates lie uniformly in the range 40–50% regularly interstratified smectite layers in all but the two most deeply buried samples (from 2271 m and 2271.9 m) for which values of 25% and 35% regularly interstratified smectite layers were obtained (Fig. 6).

Illite and illite-smectite occur as planar to undulose platelets with a sub-parallel orientation (Fig. 4b). Thin laths of clay were observed overlapping and overgrowing clay platelets in all mudrock samples (Figs. 4b–d), though in the shallower samples the laths are very short (Figs. 4b,c). These laths are indistinguishable from those observed in the sandstones (Fig. 4a). The EDS data indicate K, Al, Si, plus minor Mg and Fe, which suggest that the clay is illite but these data are not sufficiently accurate to distinguish between illite and illite-smectite. Visual estimates suggest a maximum of 1% authigenic lath-shaped clay, and an overall increase towards this value with depth (compare Figs. 4b,c with 4d). The laths are frequently partially electron-transparent in SEM images at 10 kV or above. Similar particles observed in TEM specimens have 10 Å lattice fringes and occur in packets with thicknesses of 20–100 Å. These particles are free from deformation and internal layer terminations, confirming that they are probably authigenic illite. These laths have a high proportion of face-to-edge contacts (Fig. 7a), indicating that they post-date significant compaction. They appear to grow both as overgrowths on pre-existing platelets and as discrete lath-shaped particles (Fig. 4d).

The TEM images of illite/illite-smectite in the mudrocks reveal a mass of sub-parallel packets intersecting at low angles, with the layers of one packet terminating against another along part of their length (Fig. 7b). The packets within these megacrystals (terminology of Ahn & Peacor, 1986) consist of parallel or anastomosing, wavy fringes. In ion-beam milled thin foils and conventionally microtomed samples, smectite layers often have a basal spacing of 10 Å due to dehydration during sample preparation. Consequently, layers could only be identified as smectite where collapse was not

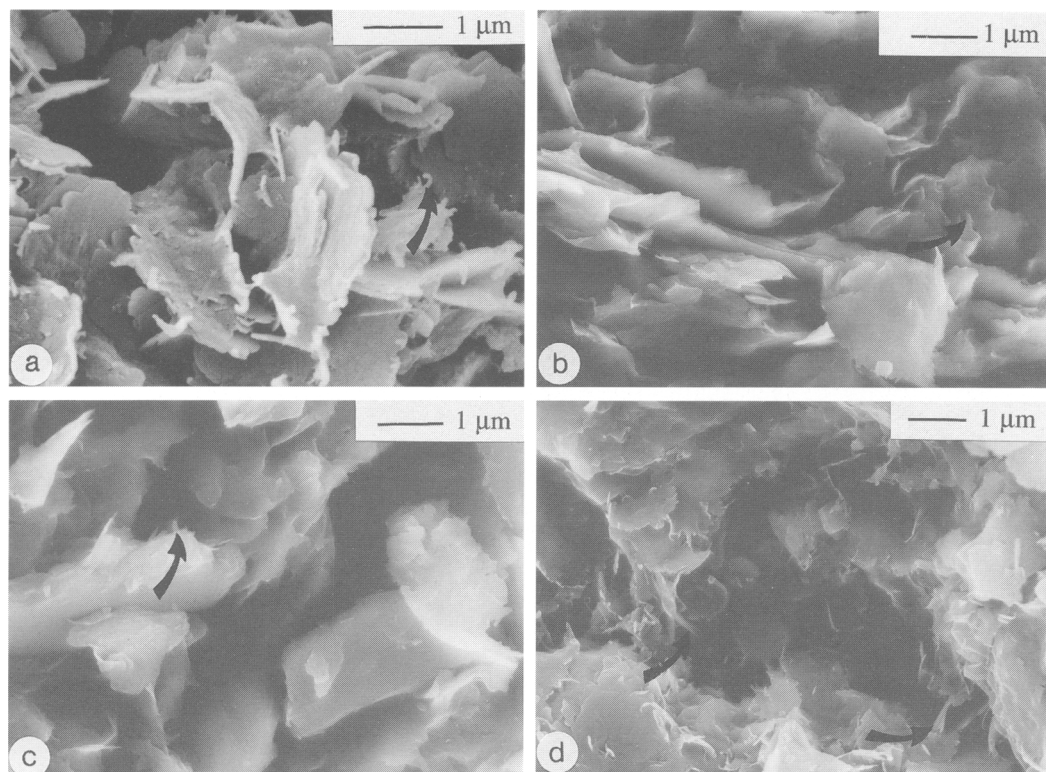


FIG. 4. FESEM micrographs of mudrocks. (a) Illitic clay with laths of clay overgrowing (arrow) clay platelets. (b) Illitic clay platelets with short, stubby, lath-shaped overgrowths (arrow), sample from 2218.9 m. (c) Illitic clay platelets with short, lath-shaped overgrowths (arrow), sample from 2251.2 m. (d) Longer, more ubiquitous laths of clay (e.g. arrows) than shown in (a) to (c), sample from 2271.9 m.

complete along the entire length of the layer (Fig. 7c), or, with more circumspection, from the undulose nature which characterizes smectite particles. Over-focusing may permit the 20 Å periodicity of R1 illite-smectite to be observed (Guthrie & Veblen, 1989; Veblen *et al.*, 1990). Unfortunately, the 20 Å periodicity is also characteristic of 2M mica. Distinction between the two needs to be made using additional textural and chemical data or knowledge of the pressure/temperature at which the mineral formed. In this instance, insufficient data are available to make the distinction.

In microtomed samples prepared by the method of Tessier (Śródoń *et al.*, 1990), 12.5–15 Å smectite, fringes intercalated with 10 Å fringes were observed. In conventionally microtomed samples fringes with periodicities of 10.5–12 Å (i.e. partially collapsed) were occasionally observed

(Fig. 7c). Within each sample examined by HRTEM, there is a spread of illite-smectite compositions which are only regularly interstratified over a few unit-cells (Fig. 7d). However, the modal composition is the same or very close to that determined by interpretation of XRD reflections. The R1 superlattice structures were mostly identified in samples for which XRD data indicate regular illite-smectite with 40–50% smectite, and R3 structures were almost exclusively identified in microtomed sections of the two deepest mudrock samples in which regular illite-smectite with 25–35% smectite was identified (Fig. 6). The XRD data indicate that the bulk of the interstratifications are regular, with a narrow compositional range, whereas the HRTEM data indicate a similar bulk composition, but with a compositional homogeneity only on a scale unlikely to be detected by XRD.

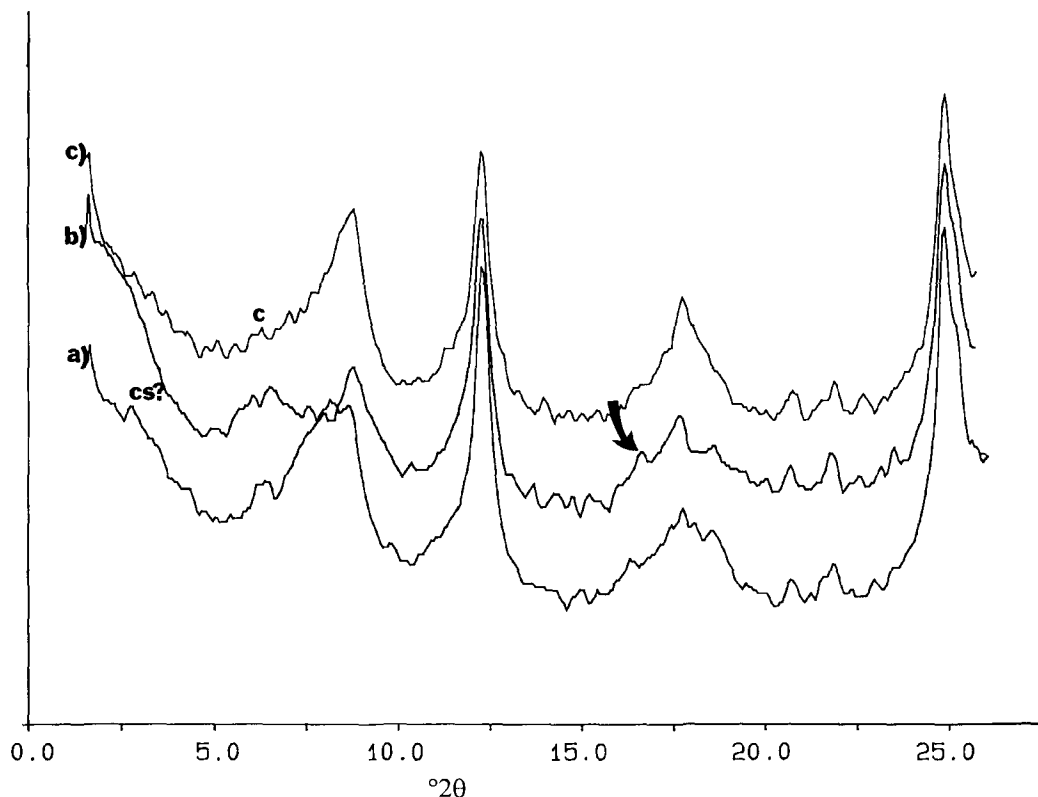


FIG. 5. Digitally smoothed XRD traces for  $<4\ \mu\text{m}$  fraction of mudrock sample from 2250.6 m; a) untreated; b) glycolated; c)  $400^\circ\text{C}$ . CS? = chlorite smectite?, C = chlorite, arrow indicates the illite-smectite 002/003 reflection used to estimate % smectite; Cu-K $\alpha$  radiation.

### Kaolinite

Kaolinite occurs predominantly as stacks of coarsely crystalline plates pseudomorphing, or intergrown with, detrital chlorite or mica, and as mono-mineralic aggregates of platelets. The pseudomorphs after mica are sometimes crushed between more rigid grains. The kaolinite is most readily observed in BSEM images (Fig. 8a). The TEM and FESEM observations confirm that discrete clay-grade kaolinite is indeed rare. Semi-quantitative estimates derived from XRD data suggest that the mudrocks (excluding the interval 2262.1–2271.28 m) typically contain 15–20% kaolinite (25–45% of the  $<4\ \mu\text{m}$  fraction). Visual estimates of the proportion of stacks and aggregates of platelets suggest 10–15%. However, the proportion of detrital kaolinite in the matrix is an unquantified factor, and 10% is, therefore, a conservative estimate.

### Chlorite

Chlorite in the shales is predominantly silt-size detrital particles. The XRD data indicate that chlorite is typically 5–15% of the clay fraction (5–10% of the bulk rock). Figure 1b shows a considerable scatter of data points but a possible decrease in chlorite with depth. Unlike the sandstone data, any depth trend in the proportion of authigenic chlorite may be concealed by the presence of detrital clay-grade chlorite.

The AEM analysis of clay-grade chlorite reveals that it commonly has a low but significant K content, indicative of a mica component. Chlorite commonly replaces biotite; the K may, therefore, be contained in relict biotite layers. This is substantiated by the HRTEM observation of 10 Å layers within some of the larger chlorite particles. Occasionally discrete packets of defect-free chlorite, 10–20 unit-cells thick, were observed by

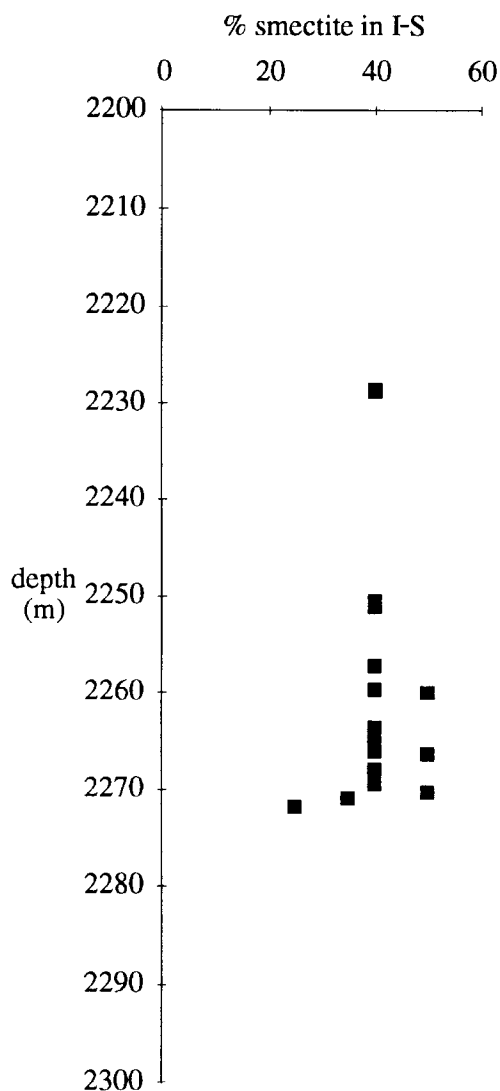


FIG. 6. Illite-smectite composition plotted against depth (mudrock data only).

HRTEM in mudrocks below 2236.5 m (EDS analysis was not possible). These chlorite particles are characteristically interleaved with defect-free, planar, illite particles of similar size; both may be neoformed but there is no conclusive evidence of this. It has not been possible to quantify depth trends in authigenic chlorite in the mudrocks. This is because it has not been possible to separate authigenic chlorite from detrital chlorite by XRD methods, and because SEM identification of

chlorite platelets is ambiguous due to contamination of EDS analyses by adjacent illitic clay platelets.

#### Non-clay minerals

The XRD data indicate that the mudrocks are typically 15–30% quartz, and visual estimates based on BSEM observation corroborate this range of values. Quartz is largely present as silt-size grains with rounded to irregular outlines; a few have straight margins and pointed terminations indicative of overgrowths (Fig. 8b). The coincidence of straight margins and pointed terminations with an open pore suggests: (1) that quartz overgrowth on most grains was inhibited by clay coatings; and (2) that the overgrowth formed *in situ* and is not reworked. Quartzite, schist and rare chert grains have been corroded. The appearance of quartz grains varies even within samples. Both diagrams, Figs. 8a,c, are from the same sample (2249.1 m). In the former, quartz grains are highly irregular in outline, whilst in the latter, grains are sub-rounded to angular but without the deep indentations seen in Fig. 8b. The grain irregularity is attributed to dissolution, possibly during pressure solution. Minor but unquantified quartz is also present in the clay fraction of all samples analysed by XRD.

The K-feldspar is generally the second most abundant grain type (2–11%, mean = 6.3%). Plagioclase (<6%, mean = 3.4%) is predominantly Ab-rich with minor partially albitized An-rich plagioclase. It is not clear whether the albitization occurred before, or during, diagenesis. Plagioclase decreases slightly with depth, whereas K-feldspar shows no depth trend (Fig. 8). The proportion of K-feldspar semi-quantitatively determined from XRD data (re-inforced by estimates from BSEM images) is 0–13% (mean = 3.3%), i.e. about half the amount in the interbedded sandstone. Feldspar is characteristically fresh but fractured (Figs. 8b,c); the rare corroded grains (Fig. 8a) may have experienced pre-depositional sericitization which predisposes them to being leached during subsequent diagenesis. The proportion of leached K-feldspar, estimated from BSEM images is about the same as point counted in sandstone thin-sections, i.e. <0.5%. The proportion of Ab-rich plagioclase semi-quantitatively determined from XRD data (and re-inforced by estimates from BSEM images) is 0–12%, with a mean value of 4.6%, i.e. the same as, or slightly more than, in the sandstones. The



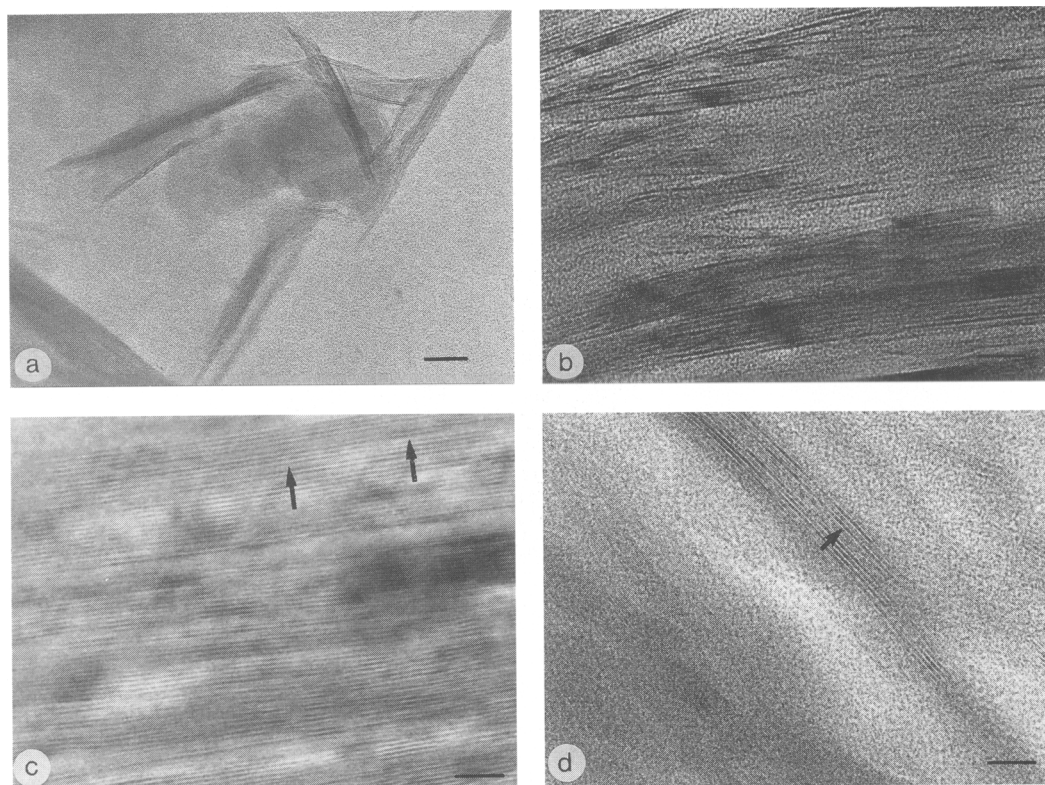


FIG. 7. High resolution bright field transmission electron micrographs in overfocus conditions (mudrocks only, all samples prepared by ultramicrotomy, without fixation of expandable layers). (a) Illite particles (laths?) free from deformation and internal layer terminations, with a high proportion of face-to-edge contacts. Scale bar = 200 Å. (b) Sub-parallel packets of 10 Å layers intersecting at low angles, with the layers of one packet terminating against another in along part of their length. Scale bar = 100 Å. (c) Partially collapsed smectite layers (arrows) have spacings  $\leq 13$  Å. Scale bar = 100 Å. (d) Illite-smectite particle with R1 structure (arrow), within overall random IS? Average composition is 50% of each layer type. Scale bar = 120 Å.

decrease in plagioclase with depth is interpreted as a decrease in detrital input, because the trend does not appear to be related to leaching or replacement.

## DISCUSSION

### *Illite and illite-smectite diagenesis*

A detrital origin for the illite and illite-smectite platelets in both lithologies is inferred from the ragged appearance of the flat to undulose platelets, and in the sandstones from the grain coating/pore-filling nature of the clay. From comparison of the clay morphologies observed here with published SEM data (e.g. Huggett, 1989; O'Brien & Slatt,

1990) the flat particles and laths are tentatively identified as illite and the undulose as illite-smectite. Where diagnostic fringes were not obtained in HRTEM images, the same tentative rule was applied as for SEM observations: parallel fringes are assumed to be illite, and anastomosing ones to be illite-smectite (Inoue *et al.*, 1988; Peacor, 1992). The FESEM observations suggest that the  $<100$  Å thick laths of illite increase in abundance with depth. These laths are interpreted as authigenic on account of their delicate morphology, and often high ratio of face-to-edge contacts, denoting that they post-date the main phase of compaction.

Previous workers (e.g. Peacor, 1992) have assumed that the authigenic lath-shaped illite,

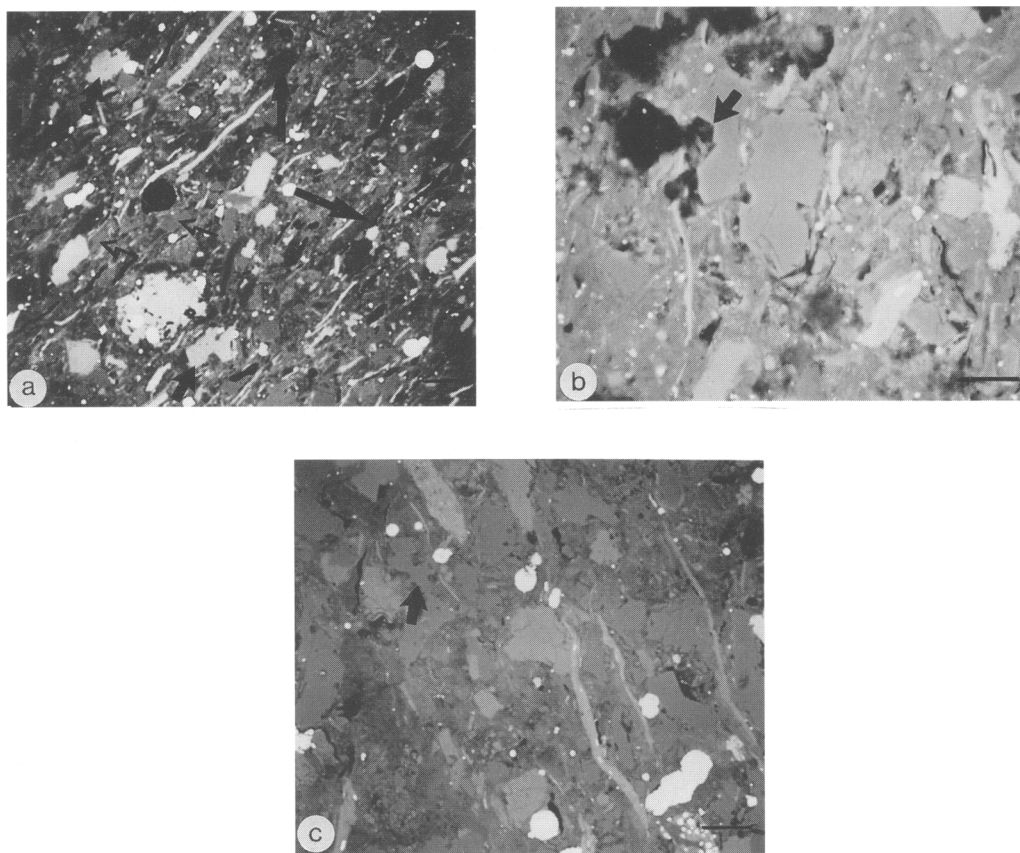


FIG. 8. The BSEM images of mudrocks: (a) quartz grains (open arrows) have been 'flattened', as a consequence of pressure solution? (2273.1 m). Conversely, much K-feldspar has been corroded to give deeply indented margins (short arrows). Dark elongate particles are kaolinite pseudomorphs after mica. Scale bar = 10  $\mu\text{m}$ . (b) Quartz grain with possible overgrowths (arrow), 2283.5 m. Scale bar = 15  $\mu\text{m}$ . (c) Quartz grains with delicately sculpted margins (e.g. arrow) suggestive of *in situ* leaching. Dark grey aggregates are kaolinite (K), light grey grains are K-feldspar (2273.1 m). Scale bar = 20  $\mu\text{m}$ .

observed in the pore space of sandstones, does not precipitate in compacted, low porosity, low permeability mudrocks. Yet in the sequence described here it has been shown not only that such illite can precipitate in mudrocks, but that it is possibly as abundant as in sandstones (i.e.  $\leq 1\%$ ). The amount of K-feldspar leaching that would be required to produce an adequate K supply to precipitate the volume of authigenic illite observed would be negligible, probably barely detectable by BSEM and certainly too small to be detected as a decrease in the proportion of K-feldspar determined by XRD (Fig. 8). Therefore there is no need, in this

instance, for K to be a mobile element, or for expulsion of K-bearing fluids from mudrock into sandstone.

### *Kaolinite*

In the sandstones, delicate booklets of kaolinite are demonstrably a product of early diagenesis, having been enclosed by calcite/ferroan calcite and quartz overgrowth cements. Subhedral kaolinite may have been corroded or reworked, though if the latter were the case it would be expected to be mixed with other clays and this is not demonstrably

Reaction (3) will yield 1 mole of kaolinite per mole of plagioclase leached. The rarity of *in situ* replacement of plagioclase by kaolinite suggests that this was a relatively unimportant reaction. Reaction (2) is sufficient to account for approximately 0.5% authigenic kaolinite through the estimated leaching of 1% K-feldspar. Allowing for the inaccuracy inherent in assessing the proportion of clay, this reaction can account for most, possibly all, the authigenic kaolinite in the sandstone. A small proportion of sandstone kaolinite does not require a feldspar source because it has replaced mica or chlorite. There is, therefore, no need for the mudrocks to supply either Al or Si for kaolinite formation in the sandstone. Calculations on the mobility of Al in subsurface fluids by Lahann (1980) and Stoessel (1987) suggest that Al is conserved during diagenesis over a distance of centimetres. The above qualitative mass balance calculations support these theoretical calculations. In the mudrock it is not clear how much kaolinite has replaced mica and how much has passively used mica, or chlorite, as a template. This uncertainty precludes any meaningful mass balance calculations for the origin of kaolinite in the mudrock.

### Chlorite

The gradual increase with depth in the proportion of authigenic chlorite in sandstones suggests that the precipitation of chlorite is controlled by depth, temperature or an increase in FeMg-rich minerals with depth. With the available data it has not been possible to assess the relative importance of these factors. The mudrock data are less clear, there being a considerable scatter of data points but a possible decrease with depth. Unlike the sandstone data, any depth trend in the proportion of authigenic chlorite may be concealed by the presence of detrital clay-grade chlorite.

The SEM and XRD data suggest that authigenic chlorite is more abundant in the sandstones than thin-section estimates suggest. This is attributed to difficulty in both identifying and point-counting clays in thin-section. Therefore, mass balance calculations for chlorite formation have not been attempted. The presence of authigenic chlorite in both lithologies suggests that the component ions for sandstone chlorite are not derived from the mudrocks, but are internally derived. In both lithologies, some *in situ* replacement of ferromagnesian mica by chlorite is inferred from the existence of mica-shaped chlorite aggregates. The slight decrease in mica with depth in the sandstones may reflect primary composition, or dissolution of unstable mica. Unlike chlorite, kaolinite shows no increase with depth, and the decrease in mica is consequently unlikely to be due to kaolinite formation. The decrease may be due to selective dissolution of FeMg-rich mica, and replacement by chlorite. The intimate association of ultra-thin illite and chlorite crystallites in the mudrocks suggests that these clay minerals have co-precipitated.

### Quartz diagenesis

Potential sources of silica for quartz overgrowth would have been dissolution of rock fragments and feldspar (both lithologies), minor replacement of feldspar, clastic lithics and mica by calcite (sandstone only, e.g. Fig. 2) and pressure solution (mudrock only). Reaction (2) will release 2 moles of silica for every mole of K-feldspar dissolved. The estimated dissolution of 1% K-feldspar will yield 2% silica for overgrowth precipitation. As the average % authigenic quartz in the sandstones is 0.5%, it may be entirely accounted for through

feldspar dissolution. Whilst there is no mass balance requirement for silica to be moved from the mudrock to the sandstone, quartz dissolution has apparently exceeded precipitation in the mudrocks. Some silica may therefore have been exported from the mudrocks. Silica export requires a means by which quartz precipitation is inhibited until the silica reaches the sandstone. Clay coatings on quartz grains may possibly inhibit internal redistribution of silica dissolved through pressure solution.

Quartz cementation is quantitatively unimportant below 85–90°C (Giles *et al.*, 1992). This is because below 100°C, both K-feldspar hydrolysis and quartz precipitation are very slow (Rimstidt & Barnes, 1980; Giles, 1987). The sampled depth range has only relatively recently entered the interval of significant quartz cementation.

### CONCLUSIONS

The detrital and authigenic mineralogy in the sandstones is almost identical to that found in the mudrocks. The principal difference is in the relative proportions of these minerals. With the possible exception of the sandstone carbonate cements, authigenic cementation may be accounted for without invoking cross-lithology flow.

Authigenic kaolinite in the sandstone is almost entirely derived through feldspar hydrolysis by internally derived acidity. In the mudrock, hydrolysis of mica has been the principal source of kaolinite. Without total organic carbon measurements, it is not possible to determine whether all the acidity for hydrolysis could be derived from within the mudrock.

The presence of authigenic chlorite in both lithologies suggests that the component ions for sandstone chlorite are not derived from the mudrocks, but are internally derived.

In the sandstone there is a steady increase in chlorite with depth, which may reflect increased alteration of ferromagnesian minerals.

Authigenic quartz in the sandstones may be entirely accounted for through feldspar dissolution. Some silica may have been exported from the mudrocks, though the mass balance does not necessitate this and by what mechanism it could be transported is unclear.

Although the proportion of authigenic illitic clay laths is low, an increase with depth is evident in the mudrocks. In the sandstones, any increase in depth

has been masked by great variability in the proportion of detrital clay on which the laths can nucleate. The critical time/temperature/K supply factors have not been resolved within the scope of this study. Illite neoformation has been such a minor process that K-feldspar leaching within either lithology is estimated to be sufficient to account for the K in the illite.

#### ACKNOWLEDGMENTS

The FESEM, TEM, ion-beam milling and ultra-microtomy were carried out by the author at the University of Queensland Centre for Microscopy and Microanalysis during a visit funded by the British Council. Additional FESEM work was carried out at the Natural History Museum (London), using a Hitachi S800. AEM work using the Philips T200 was carried out at the Micro Structural Studies Unit, University of Surrey.

#### REFERENCES

- AHN J.H. & PEACOR D.R. (1986) Transmission and analytical electron microscopy of the smectite-to-illite transition. *Clays Clay Miner.*, **34**, 165–179.
- AWWILLER D.W. (1993) Illite/smectite formation and K mass transfer during burial diagenesis of mudrocks: a study from the Texas Gulf Coast Paleocene-Eocene. *J. Sed. Pet.* **63**, 501–512.
- BOLES J.R. & FRANKS S.G. (1979) Clay diagenesis in Wilcox sandstones of southwest Texas. *J. Sed. Pet.* **49**, 55–70.
- CURTIS C.D. (1977) Sedimentary geochemistry: environments and processes dominated by involvement of an aqueous phase. *Phil. Trans. Royal Soc. A* **286**, 353–372.
- CURTIS C.D. (1978) Possible links between sandstone diagenesis and depth related geochemical reactions occurring in enclosing mudrocks. *J. Geol. Soc. Lond.* **135**, 107–117.
- GILES M.R. (1987) Mass transfer and problems of secondary porosity creation in deeply buried hydrocarbon reservoirs. *Mar. Petrol. Geol.* **4**, 188–204.
- GILES M.R. & MARSHALL J.D. (1986) Constraints on the development of secondary porosity in the subsurface: re-evaluation of processes. *Mar. Petrol. Geol.* **3**, 243–255.
- GILES M.R., STEVENSON S., MARTIN S.V., CANNON S.J.C., HAMILTON P.J., MARSHALL J.D. & SAMWAYS G.M. (1992) The reservoir properties and diagenesis of the Brent Group: a regional perspective. Pp. 289–328 in: *Geology of the Brent Group* (A.C. Morton, R.S. Haszeldine, M.R. Giles & S. Brown, editors). Geological Society, London.
- GUTHRIE G.D. JR. & VEBLEN D.R. (1989) High resolution transmission electron microscopy of mixed layer illite/smectite: computer simulations. *Clays Clay Miner.* **37**, 1–11.
- HELGESON H.C. & MURPHY W.M. (1983) Calculation of mass transfer among minerals and aqueous solutions as a function of time and surface area in geochemical processes. I Computational approach. *Math. Geol.* **15**, 109–131.
- HOWER J., ESLINGER E.V., HOWER M.E. & PERRY E.A. (1976) Mechanisms of burial metamorphism of argillaceous sediments: I Mineralogical and chemical evidence. *Bull. Geol. Assoc. Amer.* **87**, 725–737.
- HUGGETT J.M. (1989) Scanning electron microscope and X-ray diffraction investigations of mudrock fabrics, textures and mineralogy. *Scanning Microscopy*, **3**, 99–109.
- HUGGETT J.M. (1992) Petrography, mineralogy and diagenesis of overpressured Tertiary and Late Cretaceous mudrocks from the East Shetland Basin. *Clay Miner.* **27**, 480–506.
- INOUE A., VELDE B., MEUNIER A. & TOUCHARD G. (1988) Mechanism of illite formation during smectite-to-illite conversion in a hydrothermal system. *Am. Miner.* **73**, 1325–1334.
- KNOX R.W. O'B. & MORTON A.C. (1988) The record of early Tertiary N. Atlantic volcanism in sediments of the North Sea Basin. Pp. 407–419 in: *Early Tertiary Volcanism and the opening of the NE Atlantic*. Geological Society Special Publication 39 (A.C. Morton & L.M. Parson, editors). Geological Society Publishing House, Bath.
- LAHANN R.W. (1980) Smectite diagenesis and sandstone cement: the effect of reaction temperature. *J. Sed. Pet.* **50**, 755–760.
- MOORE D.M. & REYNOLDS R.C. JR. (1989) *X-ray Diffraction and the Identification and Analysis of Clay Minerals*. Oxford University Press, New York.
- O'BRIEN N.E. & SLATT R.M. (1990) *Argillaceous Rock Atlas*. Springer Verlag, New York.
- PEACOR D.R. (1992) Diagenesis and low-grade metamorphism of shales and slates. Pp. 335–379 in: *Mineral Reactions at the Atomic Scale: Transmission Electron Microscopy* (P.R. Buseck, editor). Reviews in Mineralogy **27**, Mineralogical Society of America, Washington.
- PEARSON M.J. & SMALL J.S. (1988) Illite-smectite diagenesis and palaeotemperatures in Northern North Sea Quaternary to Mesozoic shale sequences. *Clay Miner.* **23**, 109–132.
- PHAKEY P.P., CURTIS C.D. & OERTAL G. (1972) Transmission electron microscopy of fine-grained phyllosilicates in ultra-thin rock sections. *Clays Clay Miner.* **20**, 193–197.
- RIMSTIDT J.D. & BARNES H.L. (1980) The kinetics of silica-water reactions. *Geochim. Cosmochim. Acta*, **44**, 1683–1699.

- SHAW H.F. (1972) The preparation of oriented clay mineral specimens for X-ray diffraction analysis by a suction-onto-ceramic-tile method. *Clay Miner.* **3**, 349–350.
- ŠRODOŇ J. (1980) Precise identification of illite/smectite interstratifications by X-ray powder diffraction. *Clays Clay Miner.* **28**, 401–411.
- ŠRODOŇ J. (1981) X-ray identification of randomly interstratified illite/smectite in mixtures with discrete illite. *Clay Miner.* **16**, 297–304.
- ŠRODOŇ J., ANDREOLI C., ELSASS F. & ROBERT M. (1990) Direct high resolution electron microscopic measurement of expandability of mixed layer illite/smectite in bentonite rock *Clays Clay Miner.* **38**, 373–379.
- STOESSELL R. K. (1987) Mass transport in sandstones around dissolving plagioclase grains. *Geology*, **15**, 295–298.
- TESSIER D. & PEDRO G. (1982) Electron microscopy study of Na-smectite fabric – role of layer charge, salt concentration and suction parameters. *Proc. 7th Int. Clay Conf., Bologna, Pavia*, 165–176.
- TOTTEN M.W. & BLATT H. (1993) Alterations of the non-clay-mineral fraction of pelitic rocks across the diagenetic to low-grade metamorphic transition, Ouachita Mountains, Oklahoma and Arkansas. *J. Sed. Pet.* **63**, 899–908.
- VEBLEN D.R., GUTHRIE G.D., LIVI K.J.T. & REYNOLDS R.C., Jr. (1990) High resolution transmission electron microscopy and electron diffraction of mixed layer illite/smectite: Experimental results. *Clays Clay Miner.* **38**, 1–13.